J. Geogr. Sci. 2017, 27(6): 661-680
DOI: 10.1007/s11442-017-1399-z

Contributions of climate change and human activities to ET and GPP trends over North China Plain from 2000 to 2014

CHEN Xuejuan[1,2], *MO Xingguo[1,3], HU Shi[1], LIU Suxia[1,3]

1. Key Laboratory of Water Cycle and Related Land Surface Processes, Institute of Geographic Sciences and Natural Resources Research, CAS, Beijing 100101, China;
2. University of Chinese Academy of Sciences, Beijing 100049, China;
3. College of Resources and Environment/Sino-Danish Center, University of Chinese Academy of Sciences, Beijing 100049, China

Abstract: Quantifying the contributions of climate change and human activities to ecosystem evapotranspiration (ET) and gross primary productivity (GPP) changes is important for adaptation assessment and sustainable development. Spatiotemporal patterns of ET and GPP were estimated from 2000 to 2014 over North China Plain (NCP) with a physical and remote sensing-based model. The contributions of climate change and human activities to ET and GPP trends were separated and quantified by the first difference de-trending method and multivariate regression. Results showed that annual ET and GPP increased weakly, with climate change and human activities contributing 0.188 mm yr^{-2} and 0.466 mm yr^{-2} to ET trend of 0.654 mm yr^{-2}, and –1.321 g C m^{-2} yr^{-2} and 7.542 g C m^{-2} yr^{-2} to GPP trend of 6.221 g C m^{-2} yr^{-2}, respectively. In cropland, the increasing trends mainly occurred in wheat growing stage; the contributions of climate change to wheat and maize were both negative. Precipitation and sunshine duration were the major climatic factors regulating ET and GPP trends. It is concluded that human activities are the main drivers to the long term tendencies of water consumption and gross primary productivity in the NCP.

Keywords: evapotranspiration; gross primary production; contribution; process-based model; multi-regression; North China Plain

1 Introduction

Evapotranspiration (ET) is the key component that couples energy balance and water budget, and represents water consumption. Gross primary production (GPP) is the total carbon sequestration, and is so intertwined with human well-being since it is the source for food and timber production. ET and GPP are sensitive to climate and human interference (Bai *et al*.,

Received: 2016-08-17 **Accepted:** 2016-12-06
Foundation: National Natural Science Foundation of China, No.41471026; National Key Research and Development Program of China, No.2016YFC0401402
Author: Chen Xuejuan (1991–), PhD Candidate, specialized in remote sensing and eco-hydrology. E-mail: chenxj.14b@igsnrr.ac.cn
*Corresponding author: Mo Xingguo, Professor, specialized in climate and eco-hydrology. E-mail: moxg@igsnrr.ac.cn

2014; Sun *et al*., 2016; Zhang *et al*., 2013). The interactions between climate change and human activities are quite complicated and difficult to segregate, especially in ago-ecosystem (Lobell *et al*., 2011; Wang *et al*., 2016), which may affect the implementation of management practices. Separating and quantifying the contributions of climate change and human activities to ET and GPP trends is essential for understanding the impacts of climatic factors on water consumption, carbon sequestration and adaptation strategies.

Trends for ET differ between regions and ecosystems, and the driving factors are generally categorized as climate change and human activities (Li, 2014; Liu Q A *et al*., 2010; Qiu *et al*., 2008; Zhang *et al*., 2011). Studies showed that climate dominates the variability of global ET during 1982–2008, and elevated atmospheric CO_2 concentration dominates ET trends over the Asian, South American and North American regions (Shi X Y *et al*., 2013). In the area with intensive human activities, the contribution of climate change to ET trend is relative small (Bai *et al*., 2014). For example, the expansion of cropland area and the management practices explain 60.5% and 16.8% of the increased ET, while climate change accounts for 4.7% in cropland of northwest China over the past 50 years (Bai *et al*., 2014).

Vegetation productivity shows increasing trend in most parts of the world, driven by climate change and human activities (Bai *et al*., 2016; Dai *et al*., 2016; Xiao *et al*., 2015). In China, air warming explains 36.8% of the increasing trend in annual vegetation productivity during 1982–2006, while afforestation and crop yield contribute 25.5% and 15.8%, respectively (Xiao *et al*., 2015). In the Qinghai-Tibet Plateau, climate change is the main driver of the alpine grassland NPP (net primary production) increasing in the first 20-year and human activities dominate in the last 10 years during 1982–2011 (Chen *et al*., 2014). For cropland, climate change generally exerts negative effects on crop yield associated with air warming and sunshine duration decline, but these effects are usually compensated for by human activities, such as genetic techniques and crop management (Bai *et al*., 2016; Guo *et al*., 2014; Liu Y A *et al*., 2010; Lobell *et al*., 2007).

Generally, methods for quantifying the contributions of climatic and human-induced factors are categorized as field experiments (Sun *et al*., 2016; Zhang *et al*., 2013), process-based model simulations (Bai *et al*., 2016; Shi X Y *et al*., 2013) and statistical methods (Shi W J *et al*., 2013; Tao *et al*., 2008; Wang *et al*., 2016). The experimental studies need series of field measurement in a relative long time (Xiao *et al*., 2014; Zhang *et al*., 2013), which are labor-demanding and time-consuming. Process-based models (e.g., crop growth models) have been used to disentangle the contributions of different factors by comparing the results of different simulations, in which input dataset of one factor varied while holding other factors constant (Bai *et al*., 2016; Shi X Y *et al*., 2013). Process-based models can reveal mechanisms, but it is debatable that vary one factor while holding other factors constant since factors may have interrelationships with each other. Statistical models, such as multivariate regression, are easy to conduct by using historical data to calibrate relatively simple regression equations (Liu Y A *et al*., 2010; Shi W J *et al*., 2013; Wang *et al*., 2016). Statistical models can be used at site or county level (Tao *et al*., 2008; Wang *et al*., 2016), and also can be implemented at each pixel for a whole region. First difference de-trending method has been used to dissolve the issues of non-climatic trend removal when using the statistical method to evaluate the climatic contributions (Nicholls, 1997; Lobell *et al*., 2007; Tao *et al*., 2008; Veron *et al*., 2015). And the contributions of human activities can be esti-

mated by the non-climatic trends, such as the long-term changes in crop management (Lobell *et al*., 2003).

As one of the main grain production regions of China, there is great challenge for the North China Plain (NCP) to increase or maintain wheat and maize yields because of the water shortage and climate change. Researches regarding to investigating the climatic and human-induced impacts on ET or GPP of the NCP are mainly based on field experiments under specific conditions (Sun *et al*., 2016; Zhang *et al*., 2013). To better understand how ET and GPP respond to climate change and human activities at different areas of the NCP, it is imperative to separate the contributions of climatic factors and human activities for each pixel over the whole region.

In this study, a physical and remote sensing-based model (Mo *et al*., 2015; Mo *et al*., 2011) is used to estimate ET and GPP of the NCP from 2000 to 2014. By using statistical analysis methods, we aim to (1) find the dominant climatic factors associated with ET and GPP; (2) separate and quantify the contributions of climate change and human activities to ET and GPP trends.

2 Materials and methods

2.1 Study area

The North China Plain (NCP) involves Beijing, Tianjin and other five provinces, extending from latitude 32°09′N to 40°23′N and longitude 112°51′E to 122°41′E (Figure 1) with an area of 4×10^5 km^2. 85% of the NCP is cropland (Figure 1a), with a prevailing winter wheat-summer maize rotation system. It produces about 60% of wheat production and 45% of maize production for China (Zhang *et al.*, 2013).

The NCP is located in the East Asian Temperate Monsoon climate zone. The mean annual temperature is about 8–15℃ and shows an increasing trend from 2000 to 2014. The annual precipitation is about 500–1000 mm and decreases gradually from the southeast to the

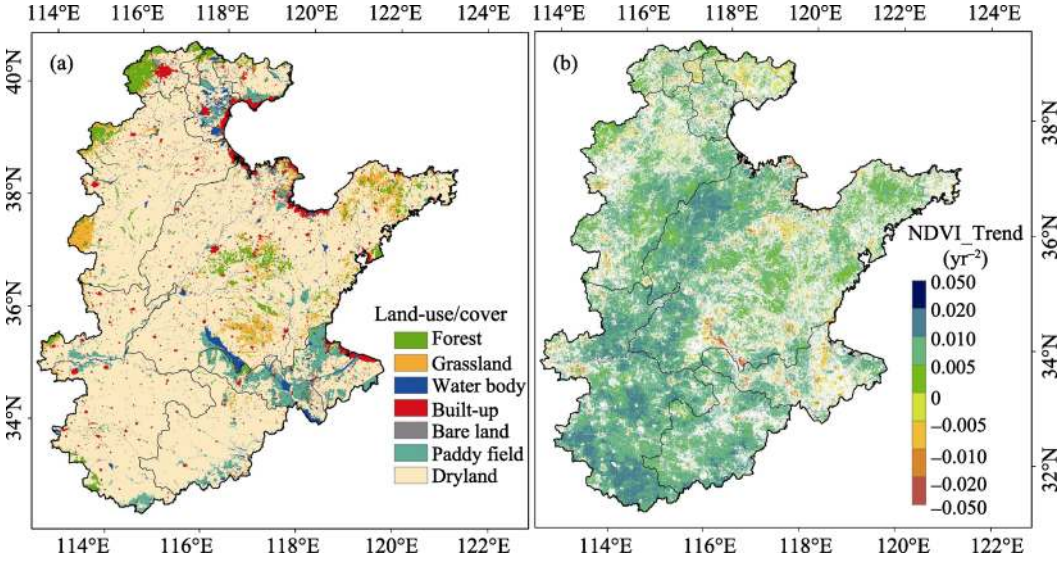

Figure 1 Land-use/cover types (a) and annual NDVI trend (P<0.05) (b) in North China Plain during 2000–2014

northwest. The precipitation, sunshine duration, relative humidity, wind speed and the reference evapotranspiration present decreasing trends (Ma *et al*., 2012; Wang *et al*., 2014), while NDVI increases significantly in most parts from 2000 to 2014 (Figure 1 b).

2.2 Model description

The remote sensing ET model used in this paper was developed by Mo *et al*. (2011, 2015). The total ET is the sum of three separated water vapor fluxes: evaporation of canopy interception, transpiration and soil evaporation. Evaporation of canopy interception equals to the potential evaporation on the wetted surface. Transpiration is estimated based on the potential transpiration and limited by water condition and temperature. Soil evaporation depends on the potential evaporation and soil exfiltration which elapsed since the day following rainfall or irrigation (Choudhury *et al*., 1998). Irrigation is set as three times in the growing season for dryland. This model uses the fraction of vegetation cover to partition the net radiation flux used for soil evaporation and transpiration. GPP is estimated by the photosynthetic active radiation intercepted by canopy and the light use efficiency which is limited by water condition and air temperature. ET and GPP of the NCP from 2000 to 2014 were simulated at daily scale for each pixel with a spatial resolution of 250 m.

2.3 Data

Land-use/cover data (Figure 1a) was provided by Data Center for Resources and Environmental Sciences, Chinese Academy of Sciences (RESDC) (http://www.resdc.cn), and converted to raster data with 250 m spatial resolution.

Daily meteorological data at 83 stations inside and around the NCP was downloaded from China Meteorological Administration website (http://data.cma.cn/). They were interpolated with the spatial resolution of 250 m by gradient inverse distance square method (Lin *et al*., 2002; Mo *et al*., 2015) which considers the effects of topographical factors.

The 16-day composite 250-m NDVI data (MOD13Q1) from 2000 to 2014 was downloaded from MODIS products website (https://lpdaac.usgs.gov/). The missing data at the beginning of 2000 was filled up by that of 2001 since vegetation fraction in winter is small and the inter-annual difference between two adjacent years can be negligible. Data with poor quality was corrected by S-G filter (Savitzky *et al*., 1964). In order to match the temporal scale of the model, the 16-day NDVI was interpolated to daily data by Lagrange polynomial method.

MODIS monthly ET (MOD16A2) and GPP (MOD17A2) products (https://lpdaac.usgs.gov/) were used to validate the simulated ET and GPP. Considering the difference of the spatial resolutions between MODIS products (1 km) and our results (250 m), simulated ET and GPP were resampled to 1 km by the bilinear interpolation method.

Eddy covariance flux measurements at Yucheng (116°38′1″E, 36°57′1″N) (2003–2005), Daxing (116°25′37″E, 39°37′16″N) (2008–2010) and Guantao (115°07′38″E, 36°30′54″N) (2008–2010) Agro-ecosystem Stations were used for ET validation. The observed ET of Yucheng Agro-ecosystem Station was provided by the Chinese Ecosystem Research Network (CERN, http://www.cerndata.ac.cn/), and that of the other two stations were provided by "Cold and Arid Regions Science Data Center at Lanzhou" (Jia *et al*., 2012; Liu S M *et al*., 2013) (http://westdc.westgis.ac.cn). For data quality control, the half-hourly data was line-

arly interpolated if data gaps in one day were less than 4.5 hours in daytime (Zhu *et al*., 2015), otherwise the data of that day were rejected.

Considering 85% of the NCP is cropland and crop yield data is available in most counties, the winter wheat and summer maize yields at county level were used as one of the data sources to validate crop GPP. The crop yield data was excerpted from provincial rural statistical yearbooks and then converted to GPP by the equation as follows:

$$GPP = \frac{Yield}{F \times R \times HI \times P} \tag{1}$$

where *Yield* is the census data at county level; *F* is the proportion of biomass above the ground to total biomass, taken as 0.9; *R* is the conversion coefficient of biomass to carbon; *HI* is the harvest index, *HI* of winter wheat is specific for each administrative district referring to Ji *et al*. (2010), and *HI* of summer maize is set as 0.49 over the whole area (Xie *et al*., 2011); *P* is the ratio of NPP to GPP (Zhang *et al*., 2009).

2.4 Analysis methods

The analysis methods include simple linear regression, the first difference de-trending method, partial correlation analysis and multivariate linear regression. These analysis methods are all performed in each grid over the whole region.

The trends of ET, GPP and climatic factors are determined by the slope of the simple linear regression model. To segregate the impacts of climatic factors and human activities, we use the first-difference de-trending method (i.e., the difference of values in one year to the previous year) to get rid of the non-climatic influences (e.g., crop management) on ET and GPP (Nicholls, 1997; Lobell *et al*., 2007; Tao *et al*., 2008; Veron *et al*., 2015).

Since the climatic factors have correlations with each other, the relationships between the de-trending climatic factors and the de-trending ET (or GPP) are quantified by the partial correlation analysis (rather than simple correlation analysis). The partial correlation analysis explores relationship of two variables independent of the influences of other factors (Nicholls, 1997; Xiao *et al*., 2015; Dass *et al*., 2016). The factor that has the highest partial correlation coefficient is identified as the dominant climatic factor.

In order to quantify the contributions of climatic factors, multivariate linear regression (Zhang *et al*., 2010) is conducted with the first differences of climatic factors as the predictor variables and the first difference in ET (or GPP) as the response variable,

$$Y_{ds} = a_1 X_{1ds} + a_2 X_{2ds} + a_3 X_{3ds} + \cdots\cdots \tag{2}$$

where, Y_{ds} is the normalized de-trended ET or GPP; a_i is the regression coefficient of each predictor; X_{ids} is the normalized de-trended climatic factor.

With the assumption that the responses of dependent variable to the climate trends and the year-to-year climate variations are similar (Nicholls, 1997; Lobell *et al*., 2007), the climatic contributions to ET (GPP) trends during 2000–2014 can be quantified by the above regression coefficients and the trends of climatic factors (Nicholls, 1997),

$$Q_c = \sum_{i=1}^{n} a_i X_{is\_trend} \tag{3}$$

$$Q_{ac} = \frac{Q_c}{Y_{s\_trend}} * Y_{trend} \tag{4}$$

where X_{is_trend} is the trend of normalized climatic factor; Q_c is the climatic contribution to the trend of normalized ET or GPP; Y_{s_trend} is the trend of normalized ET or GPP; Y_{trend} is the trend of ET or GPP; Q_{ac} is the actual climatic contribution to the trend of ET or GPP.

The surplus of the whole ET (GPP) trend and the trend caused by climatic factors is identified as the trend caused by human activities, and thus the contributions of human activities can be quantified (Lobell *et al*., 2003),

$$Q_h = Y_{s\_trend} - Q_c \tag{5}$$

$$Q_{ah} = \frac{Q_h}{Y_{s\_trend}} * Y_{trend} \tag{6}$$

where Q_h is the contribution of human activities to the trend of normalized ET or GPP; Q_{ah} is the actual contribution of human activities to the trend of ET or GPP.

In addition, the relative contributions of climate change and human activities are calculated by the equations as follows,

$$RC_c = \frac{|Q_c|}{|Q_c| + |Q_h|} \tag{7}$$

$$RC_h = \frac{|Q_h|}{|Q_c| + |Q_h|} \tag{8}$$

where RC_c and RC_h are the relative contributions of climate change and human activities, respectively.

2.5 Selection of climatic predictors

The sunshine duration (or radiation), mean daily temperature, precipitation, vapor pressure deficit (or humidity) and wind speed are the key climatic factors that influencing ET (Ukkola *et al*., 2013; Cao *et al*., 2014). In addition to these factors (except for wind speed), diurnal temperature range has also been reported as the driving climatic force of GPP (Roderick *et al*., 2001; Zhang *et al*., 2013; Dass *et al*., 2016). However, due to the strong auto-correlations between some of these factors, it is fallacious to conduct multivariate regression model with all these factors being the predictors. As the simple correlation coefficients of every two de-trended climatic factors for each grid shown in Figure 2, the sunshine duration (SD), diurnal temperature range (DTR) and vapor pressure deficit (VPD) are significantly correlated with each other in more than 95% of the areas of the NCP. We will not consider DTR and VPD as the predictors in our study. The subsequent analysis will focus on the relationships between ET (or GPP) and the screened factors (SD, Ta, PPT and WS). Considering that wind is the aerodynamic demand for evaporation but has no direct effect on GPP, we will take wind speed as one of the main climatic predictors only for ET regression.

3 Results and analysis

3.1 Model validation

Figures 3a, 3b and 3c show the comparisons between daily ET estimations and observations at three eddy covariance flux sites across the NCP. In order to reduce the uncertainty that comes from the effects of flux footprint and geographical accuracy of remote sensing

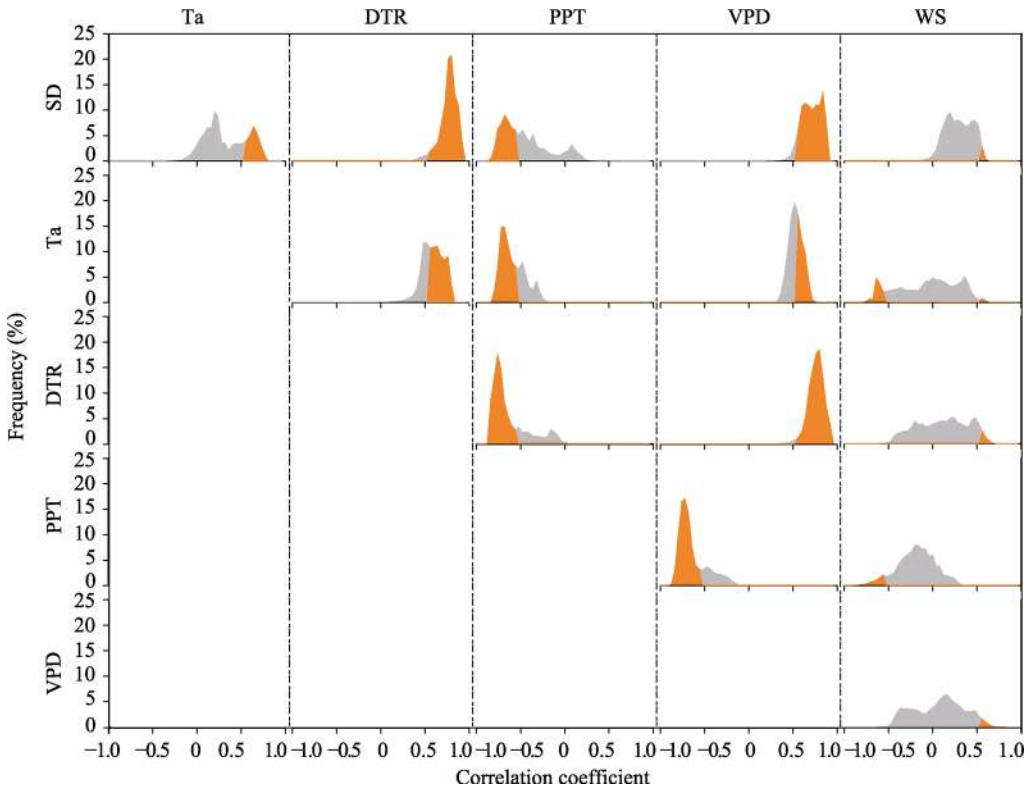

Figure 2 The probability density functions (PDF) of the spatial distributions of simple correlation coefficients between every two de-trended climatic factors. PDF in gray color represents all the grids, and PDF in orange color represents the grids which are under 95% level significant. (SD: sunshine duration; Ta: mean temperature; DTR: diurnal temperature range; PPT: precipitation; VPD: vapor pressure deficit; WS: wind speed.)

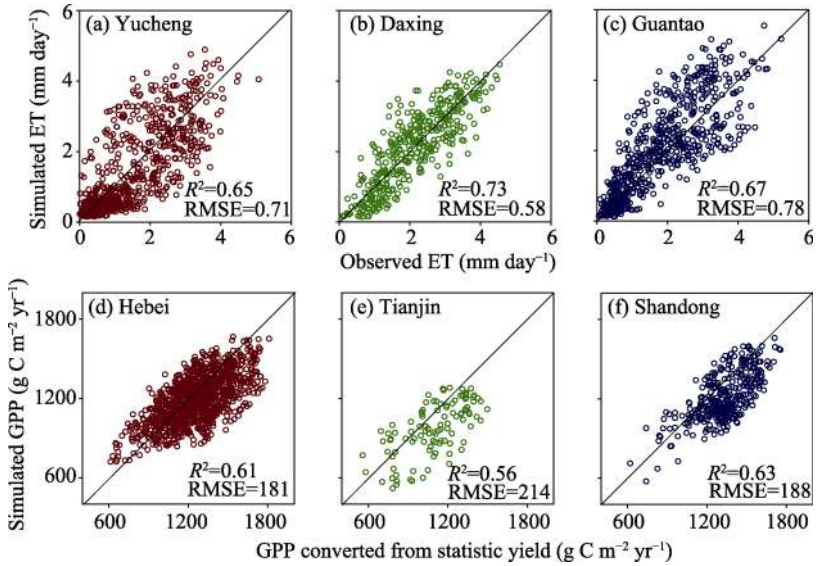

Figure 3 Comparisons between simulated daily ET and measured ET by eddy covariance in three flux towers, Yucheng: 2003–2005 (a), Daxing: 2008–2010 (b), and Guantao: 2008–2010 (c); and comparisons between simulated crop GPP and retrieved GPP by available statistic grain yields at county level during 2000–2014 in three provinces of Hebei (d), Tianjin (e), and Shandong (f)

data, the estimated ET were averaged over the 3×3 pixel subsets (250×250 m^2) around the flux sites (Wang *et al*., 2010). In general, the model performed fairly well in estimating ET, with the coefficients of determination (R^2) being 0.65 (P<0.05), 0.73 (P<0.05) and 0.67 (P<0.05), and the root mean square errors (RMSE) being 0.71, 0.58 and 0.78 mm day^{-1} for Yucheng, Daxing and Guantao sites, respectively. This model has also given a reliable results on ET estimations in paddy field (Taoyuan) and grassland (Xilinhot sites) (Mo *et al*., 2015), and the estimated ET of China were consistent with those estimated by water balance method (Mo *et al*., 2015). Figures 3d, 3e and 3f show the comparisons between simulated crop GPP and retrieved GPP by statistic grain yields at county level with R^2 of 0.61 (P<0.05), 0.56 (P<0.05) and 0.63 (P<0.05), and RMSE of 181, 214 and 188 g C m^{-2} yr^{-1} for Hebei, Tianjin and Shandong provinces, respectively. The scatters are all around 1:1 line. These indicate that the simulated GPP is in good agreement with the yield converted GPP.

ET and GPP were compared with MODIS products in forest, grassland and cropland at monthly scale (Figure 4). All correlation coefficients are larger than 0.9, which means that the seasonal patterns of our simulations are consistent with the MODIS products. However, the normalized standard deviations and the RMSE for cropland are relative higher than that of forest and grassland. This is because in cropland, MODIS-ET algorithm did not consider irrigation (Mu *et al*., 2011), and MODIS-GPP is usually overestimated in non-growth season but underestimated in growth season (Gao *et al*., 2014; Liu *et al*., 2015; Liu *et al*., 2014). Study stated that annual MODIS-GPP over irrigated cropland in the NCP only accounts for about 1/5–1/3 of the ground truth GPP, which is attributed to the underestimations of maximum light use efficiency (LUE) and leaf area index (LAI, MOD15) (Zhang *et al*., 2008). In our model, we considered irrigation for cropland and parameterized the minimum stomatal resistance for each plant functional type to calculate ET, and optimized the maximum LUE for estimating GPP according to recent study (Zhang *et al*., 2016). By this way, the accuracy of ET and GPP estimation has been improved.

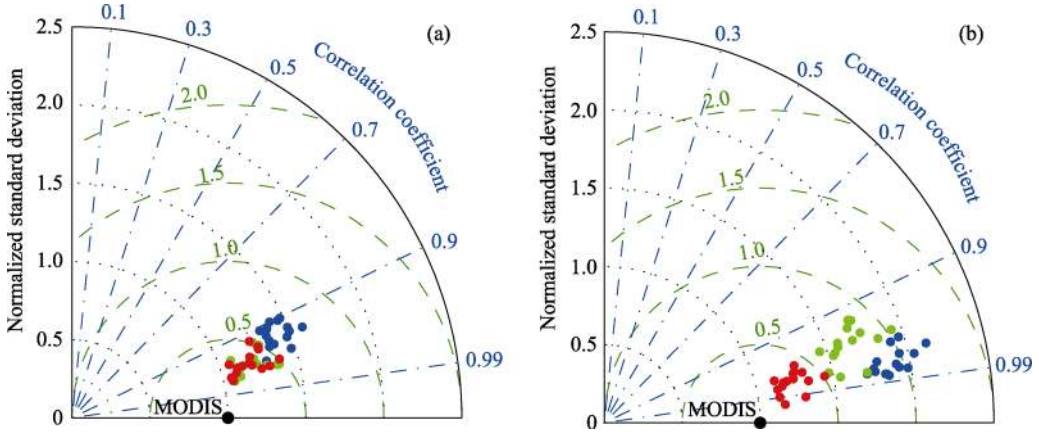

Figure 4 Taylor diagram of the comparisons between monthly simulated ET and MODIS-ET (a); simulated GPP and MODIS-GPP (b) over cropland (blue), forest (green) and grassland (red) during 2000–2014

3.2 Spatiotemporal variations of ET and GPP

Mean annual ET and GPP averaged across the NCP from 2000 to 2014 are 600 mm yr^{-1} and

1196 g C m^{-2} yr^{-1}, respectively, and ET and GPP of drought year (2000, 2001, 2002 and 2006) are lower than the multi-year mean value, as shown in Figure 5. Regional averaged ET and GPP increase with the trends of 0.654 mm yr^{-2} and 6.221 g C m^{-2} yr^{-2} (P<0.1) from 2000 to 2014. The PDFs (probability density functions) of ET are symmetrically distributed across the blue line with concentrated variation range, and the coefficients of variation (CV) for the spatial distributions of ET are about 0.2. However, GPP shows relative larger spatial difference with variation range from 0 to 2200 g C m^{-2} yr^{-1} and the modes of PDF being larger than the mean values. In addition, the CVs of GPP are larger than 0.3 and show a significantly (P<0.05) increasing trend (Figure 5).

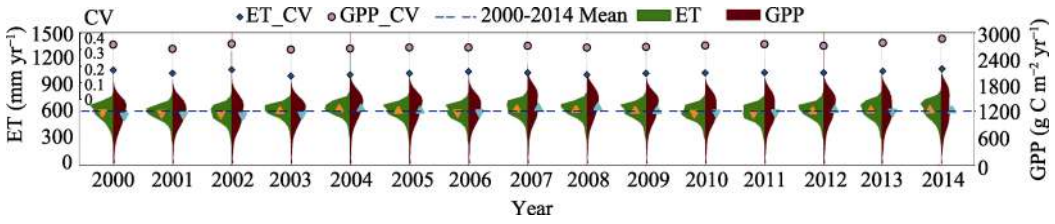

Figure 5 Probability density functions (PDF) and mean values (triangle symbol, upward or downward triangle means larger or smaller than the multi-year mean value) of the spatial distributions of ET and GPP from 2000 to 2014. ET is shown on the left side in green and GPP is shown on the right side in red. The blue horizontal line shows the multi-year mean value averaged over the whole region for ET and GPP. The series of blue rhombus and pink circles represent the variation coefficients of ET and GPP, respectively.

Generally, ET and GPP decrease with latitude and altitude (Figure 6a and 6b). They are high in the southern and central cropland, especially in Jiangsu and Anhui provinces where ET and GPP are higher than 700 mm yr^{-1} and 1400 g C m^{-2} yr^{-1}. About 16% (P<0.05) and 29.2% (P<0.05) of the region show significant increasing trends while 9.5% (P<0.05) and 8.8% (P<0.05) show significant decreasing trends for ET and GPP, respectively (Table 1). Decreasing ET and GPP mainly occur in the western and northern parts of the plain and some areas of Shandong province (Figure 6c and 6d). Trends for ET averaged over the significantly decreasing (P<0.05), insignificantly decreasing (P>0.05), insignificantly increasing (P>0.05) and significantly increasing (P<0.05) regions are –6.86, –1.79, 2.03 and 5.71 mm yr^{-2}, while that for GPP are –28.66, –7.29, 8.58, and 24.04 g C m^{-2} yr^{-2}, respectively (Table 1).

3.3 Dominant climatic factors of ET and GPP

Based on the de-trending data series which removed the impacts of non-climatic factors, the dominant climatic factors of ET and GPP are identified by the highest partial correlation coefficients for each grid of the NCP (Figure 7). It is shown that annual ET variations have the largest partial correlation coefficients with precipitation variations in about 42.9% of the region which mainly distributes in the central and northern part (Figure 7a). The western piedmont plain and the northern part of Jiangsu province are widely dominated by temperature. Sunshine duration plays the major role in southwest NCP, mainly in central Henan and north Anhui province. Areas discretely dominated by wind speed only accounts for 6.2% of the NCP. In wheat growing stage, precipitation dominates ET in the largest area, followed by temperature, sunshine duration and wind speed (Figure 7b). In maize growing stage, ET is dominated by precipitation and sunshine duration in 60.7% areas of the NCP (Figure 7c).

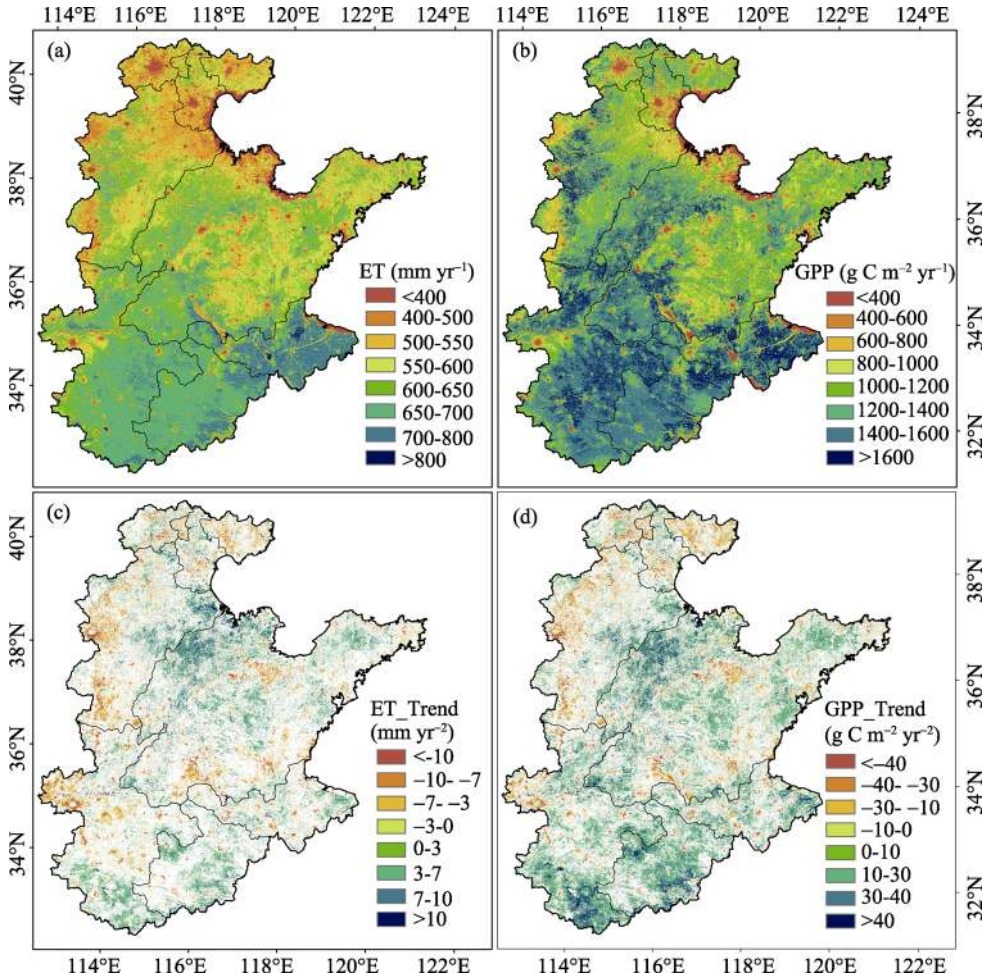

Figure 6 The spatial distributions of annual mean ET (a); annual mean GPP (b); trends of annual ET (P<0.05) (c) and trends of annual GPP (P<0.05) (d) over the North China Plain from 2000 to 2014

Table 1 The area proportions and mean values of ET and GPP trends

	Area_ET trend (%)	ET_trend (mm yr^{-2})	Area_GPP trend (%)	GPP_trend (g C m^{-2} yr^{-2})
Decrease (P<0.05)	9.5	–6.864	8.8	–28.655
Decrease (P>0.05)	29.5	–1.794	22.7	–7.289
Increase (P>0.05)	45.1	2.034	39.3	8.579
Increase (P<0.05)	16.0	5.712	29.2	24.041

The role of precipitation indicates that water conditions are more critical than energy for evapotranspiration in the water-shortage NCP at annual scale, while in maize growing stage when precipitation is relative abundant, the role of sunshine duration is fairly important.

In most area, the partial correlation coefficients between de-trended annual GPP, GPP in wheat growing stage and climatic factors (Figures 7d and 7e) are not significant. Annual GPP in 17.1%, 14.4% and 12.2% areas of the NCP is dominated by precipitation, temperature and sunshine duration, respectively. In wheat growing stage, it is conspicuous that temperature dominates GPP, especially in western piedmont region (Figure 7e). In maize growing

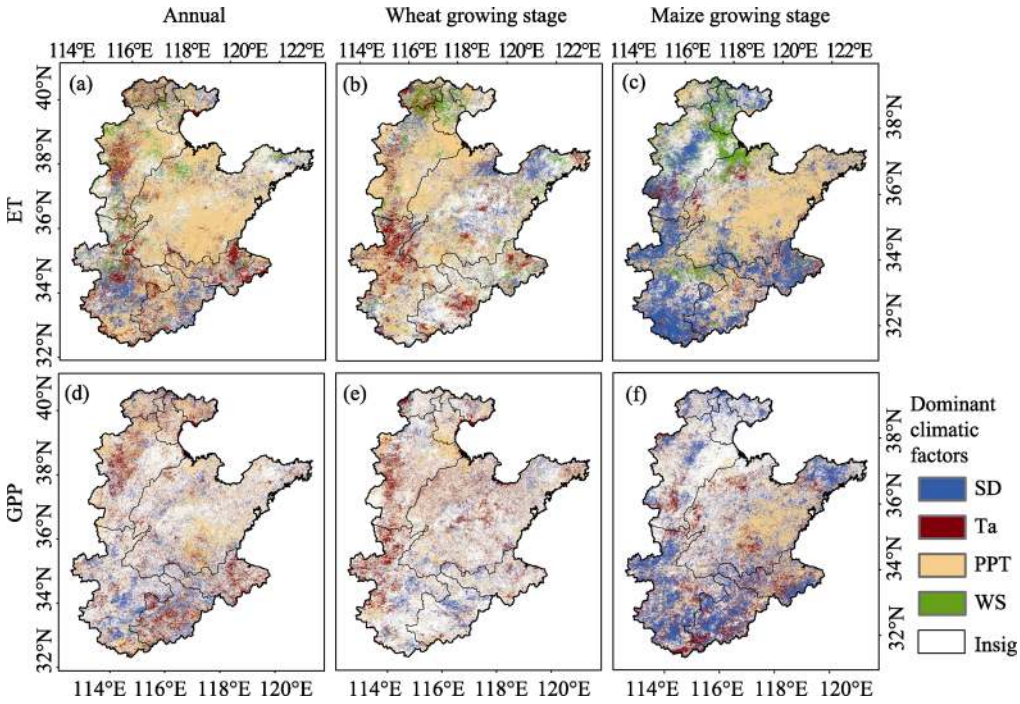

Figure 7 Spatial distributions of dominant climatic variables of annual ET (a), ET in wheat growing stage (b), ET in maize growing stage (c), annual GPP (d), GPP in wheat growing stage (e), and GPP in maize growing stage (f) (P<0.05) from 2000 to 2014 after removing the non-climatic influences. (The white color represents that the partial correlations between ET (or GPP) and climatic factors are insignificant. Wheat growing stage: during Oct, Nov, Dec, Jan, Feb, Mar, Apr and May; Maize growing stage: during Jun, Jul, Aug and Sep.)

stage (Figure 7f), the effect of sunshine duration is prominent. SD dominates 26.8% of the NCP discretely, except for the mountain area in south Shandong province in which precipitation plays a major role.

Therefore, precipitation and sunshine duration are the dominant climatic factors of ET and GPP.

3.4 Contributions of climate change and human activities to ET and GPP trends

3.4.1 Relative contributions of climate change and human activities

The relative contributions of climate change and human activities to ET and GPP trends for each grid in the whole region are shown in Figure 8. Generally, human activities contribute more than climate change to both ET and GPP. Averaged over the whole region, the relative contributions of climate change to ET and GPP are 39.5% and 26%, while those of human activities are 60.5% and 74%, respectively. Along the Yellow River and in the forests of northwest NCP, ET trends are obviously dominated by climate change, of which the contributions are greater than 50%. The relative contributions of human activities to GPP are more than 90% in a large part of cropland, which highlights the role of agricultural management practices.

3.4.2 Actual contributions of climate change and human activities

The actual contributions of climate change and human activities to ET and GPP trends are

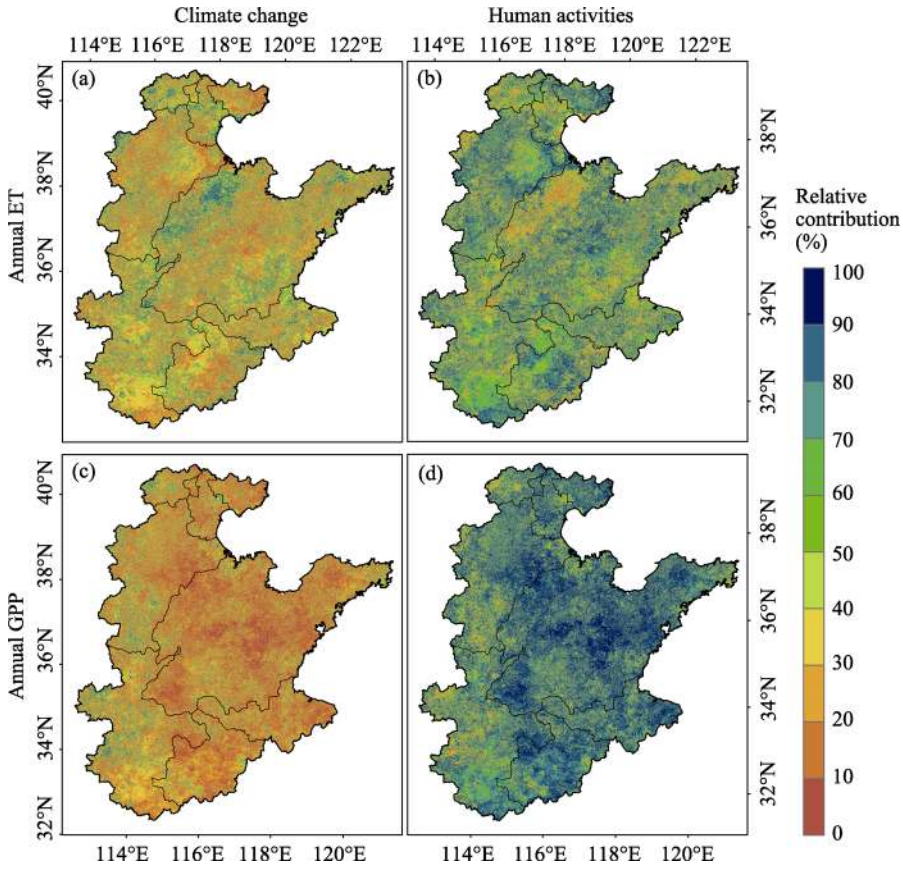

Figure 8 Relative contributions of climate change and human activities to annual ET and GPP trends. (The sum of the relative contributions equals to 100%.)

summarized in Table 2. Climate change contributes 0.188 mm yr^{-2} (28.8%), and human activities contribute 0.466 mm yr^{-2} (71.2%) to ET trend of 0.654 mm yr^{-2}. ET trend over the significantly (P<0.05) changing area (as shown in Figure 6c) is 1.045 mm yr^{-2}, of which climate change contributes 0.416 mm yr^{-2} (39.8%), and human activities contribute 0.630 mm yr^{-2} (60.2%). In the area ET shows significantly increasing trend (P<0.05), climate change and human activities contribute 0.515 mm yr^{-2} (9%) and 5.197 mm yr^{-2} (91.0%), respectively. In the area ET decreases significantly (P<0.05) with the trend of –6.864 mm yr^{-2}, the trends induced by climate change and human activities are 0.247 mm yr^{-2} and –7.111 mm yr^{-2}, respectively.

For GPP trend, climate change contributes –1.321 g C m^{-2} yr^{-2} and human activities contribute 7.542 g C m^{-2} yr^{-2} in the whole region. GPP trend averaged over the significantly (P<0.05) changing region (as shown in Figure 6d) is 11.863 g C m^{-2} yr^{-2}, of which the changes induced by climate change and human activities are –1.876 g C m^{-2} yr^{-2} and 13.739 g C m^{-2} yr^{-2}, respectively. As for the significantly increasing areas (P<0.05), climate change contributes –2.169 g C m^{-2} yr^{-2} and human activities contribute 26.210 g C m^{-2} yr^{-2}, which prompt the GPP trend of 24.041 g C m^{-2} yr^{-2}. For the significantly decreasing areas (P<0.05) with the trend of –28.655 g C m^{-2} yr^{-2}, the contribution of human activities accounts for –27.752 g C m^{-2} yr^{-2}.

Table 2 Mean actual contributions of climate change and human activities to annual ET trends (mm yr^{-2}) and GPP trends (g C m^{-2} yr^{-2})

Zones	ET trend	Q_{ac} to ET trend	Q_{ah} to ET trend	GPP trend	Q_{ac} to GPP trend	Q_{ah} to GPP trend
A	0.654	0.188	0.466	6.221	–1.321	7.542
B	1.045	0.416	0.630	11.863	–1.876	13.739
C	5.712	0.515	5.197	24.041	–2.169	26.210
D	–6.864	0.247	–7.111	–28.655	–0.903	–27.752

Note: A represents the whole area of the NCP; B represents the area where ET or GPP trends are significant; C and D represent the areas that ET (or GPP) shows significantly increasing trend and significantly decreasing trend, respectively. Q_{ac} and Q_{ah} are the actual contributions of climate change and human activities as defined in section 2.4.

ET trends show difference among land use types (Figure 9a). Areas with decreasing ET trends are mainly occupied by forest and built-up land (Figure 9a). In these two land use types, human activities contribute negatively to ET trends, which offset the increasing trends arose by climate change. Except for these two types, the contributions of human activities to ET trends are all positive. In grassland, annual ET shows increasing trend, climate change and human activities both show positive contributions in which climate change plays a dominant role (Figure 9a). In water body and cropland, human activities have positive contributions to ET while climate change contributes negatively. ET of winter wheat increases 0.802 mm yr^{-2}, in which climate change and human activities contribute –0.110 mm yr^{-2} and 0.912 mm yr^{-2}, respectively (Figure 9a). However, for summer maize, ET shows decreasing trend of –0.028 mm yr^{-2} with climate change contributing negatively (–0.163 mm yr^{-2}) and human activities contributing positively (0.135 mm yr^{-2}) (Figure 9a).

For GPP trends, contributions of climate change are negative and that of human activities are positive except for grassland. In grassland, contributions of climate change and human activities both are positive (Figure 9b). Human activities contribute dominantly to GPP increases in grassland, forest and cropland. For cropland, trend of GPP in maize growing stage is 0.103 g C m^{-2} yr^{-2}, in which climate change and human activities contribute –1.712 and 1.815 g C m^{-2} yr^{-2}, respectively (Figure 9b). In wheat growing stage, the negative contribution of climate change is weak and human activities dominate the increase of GPP. GPP of wheat increases with trend of 7.097 g C m^{-2} yr^{-2}, in which –0.099 g C m^{-2} yr^{-2} is attributed

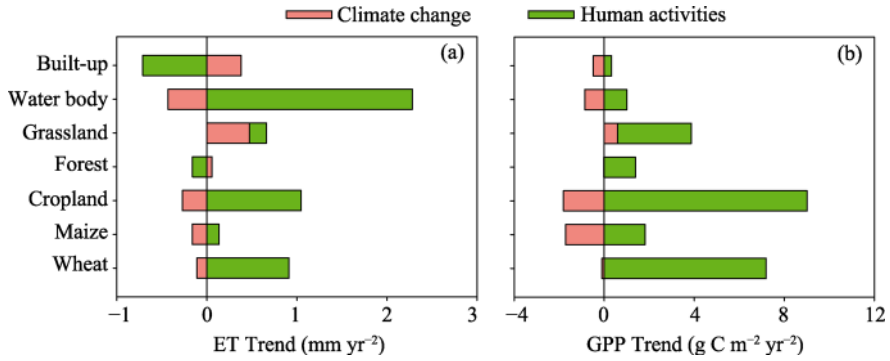

Figure 9 Actual contributions of climate change and human activities to ET and GPP trends in different land use types. (We further distinct the winter wheat and summer maize in cropland; GPP of water body is for the vegetation in wetland and benchland.)

to climate change and 7.196 g C m^{-2} yr^{-2} is attributed to human activities (Figure 9b).

In general, human activities dominate ET and GPP trends. For the regional average ET, climate change and human activities both have positive impacts, while for the regional average GPP, climate change has negative effect but this effect is eventually offset by the dominant positive impact of human activities. For cropland, the contributions of climate change are negative while that of human activities are positive. The negative climatic contributions on wheat are relative small than that on maize.

4 Discussion

4.1 ET, GPP and their trends

The annual mean ET of the NCP is 600 mm yr^{-1}, which is similar to the result of Lei *et al*. (2010) in which annual ET over an irrigated cropland in the NCP is 595 mm in the period of 2005–2006 and 609 mm in the period of 2006–2007, respectively. But compared with MODIS-ET whose annual mean value is 485 mm, our result is much higher. The simulated ET that is higher than MODIS-ET mainly distributes in the central and northern parts of the NCP (Figure 10c) where NDVI is larger than 0.25 (Figure 11a). In these areas, crop irrigation is prevailing (Mo *et al*., 2011). But MODIS-ET algorithm neglects the impact of irrigation. This may be the main reason for the difference between our simulated ET and MODIS-ET.

It is reasonable that simulated annual mean GPP is 1196 g C m^{-2} yr^{-1} since GPP in pure cropland approaches about 1500 g C m^{-2} yr^{-1} (Wang *et al*., 2015; Zhang *et al*., 2008). By contrast, annual mean MODIS-GPP of the NCP is only 800 g C m^{-2} yr^{-1}. Large difference was also observed between estimated GPP (Xiao *et al*., 2010) and MODIS-GPP in United States, particularly for croplands in the Midwest, in which estimated annual GPP and MODIS-GPP are ~1200–1500 and ~700 g C m^{-2} yr^{-1}, respectively. MODIS-GPP that is lower than our simulation mainly distributes in the central and western NCP (Figure 10f) where the land use type is mainly cropland (Figure 1a) and NDVI is larger than 0.3 (Figure 11b). This is mainly because the maximum light use efficiency is underestimated (only 0.68 g C MJ^{-1}) for cropland in MODIS algorithm (Xiao *et al*., 2010; Zhang *et al*., 2008). In addition, MODIS-GPP is overestimated when NDVI is lower than 0.3 (Figure 11b). These support the view that MODIS-GPP is underestimated at high productivity and overestimated at low productivity areas (Turner *et al*., 2006).

In our study, annual ET exhibits increasing trends. Study based on measured data also indicated that actual water use of the NCP increased in recent three decades (Zhang *et al*., 2011). In the irrigated croplands of America, ET also showed increasing trend (Jaksa *et al*., 2015). However, trend in annual MODIS-ET of the NCP is negative as shown in Figure 12a, which is mainly due to the ET decline in maize growing stage. The correlation coefficient of our predicted annual ET and the significantly increased NDVI (trend=0.004 (P<0.01)) is 0.51 (P<0.05), but only 0.06 for MODIS-ET and NDVI. Therefore, our estimated ET that shows increasing trend captured the vegetation dynamic preferably compared to MODIS-ET. Although there are discrepancies in GPP magnitudes between our simulations and MODIS product, trends of them are similar as shown in Figure 12b. MODIS-GPP and simulated GPP both have good relationships with NDVI with the correlation coefficients being 0.83 (P<0.01) and 0.75 (P<0.01), respectively.

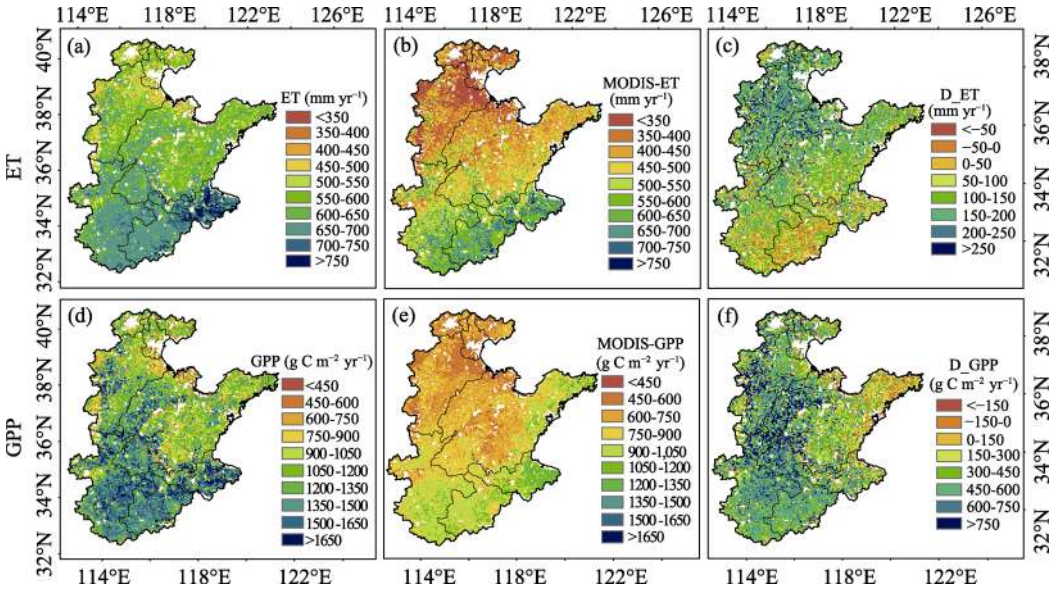

Figure 10 Spatial distributions of annual mean simulated ET (a), annual mean MODIS-ET (b), difference between annual mean simulated ET and annual mean MODIS-ET (c), annual mean simulated GPP (d), annual mean MODIS-GPP (e), difference between annual mean simulated GPP and annual mean MODIS-GPP (f)

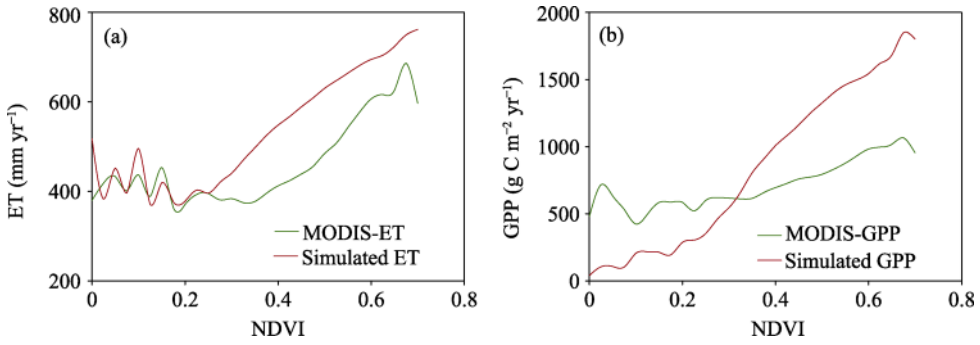

Figure 11 Variations of annual mean ET (a) and GPP (b) with the pattern of NDVI

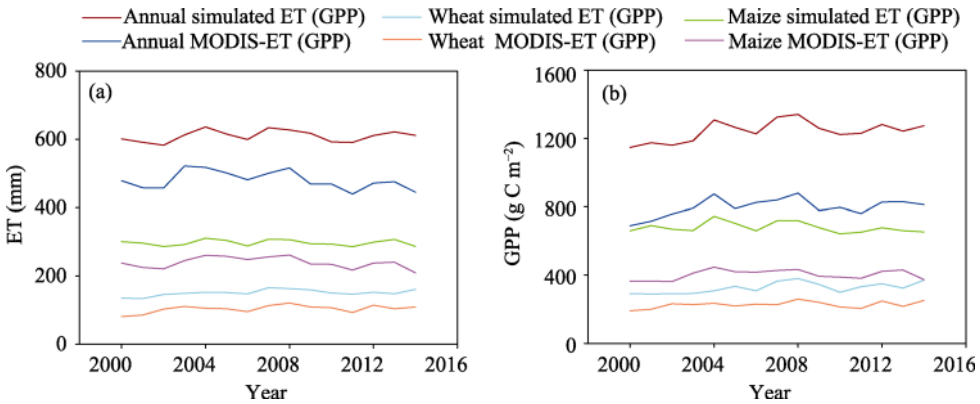

Figure 12 Changes of ET (a) and GPP (b) in the North China Plain from 2000 to 2014 (Mean ET and GPP are all averaged over the areas where MODIS products have valid values.)

4.2 Sensitivities of ET (GPP) to climatic variables

When using the first-difference de-trending method to remove the non-climatic influences and then assessing the contributions of climate change by the linear regression model, there is an assumption that the responses of ET (or GPP) to the trends of climatic factors and the year-to-year variations are similar (Nicholls, 1997; Lobell *et al*., 2007). That means ET (or GPP) and climatic variables are assumed to be linearly associated, which may introduce some biases.

The sensitivities of ET (or GPP) to climatic factors are analyzed to illustrate this issue. If ET (or GPP) and climatic variables are linearly associated, the sensitivities of ET (or GPP) to climatic factors should be the same before and after climate change. If they are not linearly associated, the sensitivities are different and the differences of the sensitivities indicate the biases arose from the non-linear relationships. By comparing the sensitivities of ET (or GPP) to climatic factors under the present climate condition and the changed climate condition, it was found that the sensitivity of ET to Ta increasing 1℃ when WS decreasing 20% has the largest difference which is shown as the orange circle in the fourth column of Figure 13a. For GPP (Figure 13b), the difference of the sensitivities to SD under different Ta conditions is the largest. Generally, the differences of the sensitivities of ET to SD (or Ta, PPT, WS) under different climatic conditions are all less than 1%, and that of GPP are all less than 1‰, which means that the biases arisen by the non-linear associations are small and negligible. Therefore, the relationships between ET (or GPP) and climatic factors can be assumed linear, and the sum of the effects of climate variables can represent their interactive roles in affecting ET or GPP.

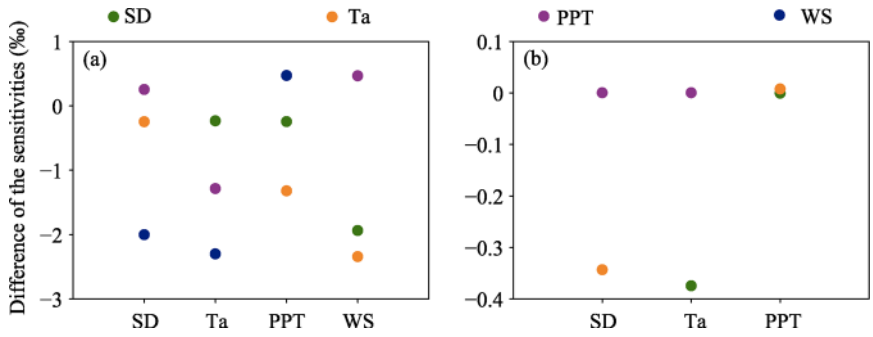

Figure 13 Differences of the sensitivities of ET (a) and GPP (b) to each climate factor under different climatic conditions. (Specifically, assume that the sensitivity of ET to Ta increasing 1℃ is A, and the sensitivity of ET to Ta increasing 1℃ when SD decreases 20% is B. The difference of A and B is shown as the orange circle in the first column of (a). The differences of the sensitivities of ET (or GPP) to other factors are estimated similarly. Changes of SD, PPT and WS are set as decreasing 20%, while change of Ta is set as increasing 1℃ according to the climatic conditions of the North China Plain.)

4.3 Impacts of climate change and human activities on crops

Generally, technology advances and crop management practices adapted by farmers can mitigate and offset the disadvantages of climate change for crop productivity. For example, Lobell *et al*. (2007) indicated that global yields of wheat and maize response negatively to increased temperatures, but these negative impacts are smaller than the impacts of technol-

ogy. In China, Guo *et al*. (2014) demonstrated that technological progress contributes dominantly to maize yield increase during 1981–2010, although climate change has negative effects on maize. In this study, our results support this view that crop productivities increase over the NCP during 2000–2014, which are contributed mainly by human activities.

Table 3 Trends of climatic factors averaged over cropland from 2000 to 2014

Trend	SD	Ta	PPT	WS
Wheat growing stage	0.010	0.007	–0.126	–0.046**
Maize growing stage	–0.049*	–0.001	–0.593	–0.043**

Note: ** indicates $P<0.05$; * indicates $P<0.1$

In the NCP, we find that climate change has negative impacts on both wheat and maize for ET and GPP, but the effects on wheat are relative small. Climate change influences terrestrial eco-hydrological process by altering the spatiotemporal distribution of precipitation, available energy, and air temperature. Positive response of crop yield to sunshine duration has been concluded by the experimental researches (Sun *et al*., 2016; Zhang *et al*., 2013). In maize growing stage, sunshine duration decreases significantly (Table 3), which reduces surface available energy, photosysthesis rate and biomass accumulation, and consequently causes water consumption and crop yield decrease (Bai *et al*., 2016; Liu *et al*., 2005). Furthermore, temperature in wheat growing stage shows weakly increasing trend (Table 3), which may accelerate evapotranspiration and help winter wheat avoid freezing disaster. In addition, precipitation in wheat growing stage and maize growing stage both show decreasing trend, but the decreasing magnitude of PPT in maize growing stage is larger than that in wheat growing stage (Table 3). These may be the major reasons for the different magnitudes of the negative effects of climate change on wheat and maize.

5 Conclusions

Based on a remote sensing and physical model, the spatiotemporal patterns of ET and GPP were estimated from 2000 to 2014 over the NCP with a 250-m resolution. Dominant climatic factors of ET and GPP were identified by the partial correlation analysis, and the contributions of climate change and human activities to ET and GPP trends were separated and quantified by the first-difference de-trending method and multivariate regression.

Annual mean ET and GPP averaged over the NCP from 2000 to 2014 were increasing with trends of 0.654 mm yr^{-2} and 6.221 g C m^{-2} yr^{-2} ($P<0.1$), respectively. About 16% and 29.2% of the area in the NCP showed significantly increasing trends while 9.5% and 8.8% showed significantly decreasing trends for annual ET and GPP, respectively. The relative contributions of climate change and human activities to ET trends were 39.5% and 60.5%, and those to GPP trends were 26% and 74%, respectively. Climate change and human activities contributed 0.188 mm yr^{-2} and 0.466 mm yr^{-2} to ET trend of 0.654 mm yr^{-2}, and –1.321 g C m^{-2} yr^{-2} and 7.542 g C m^{-2} yr^{-2} to GPP trend of 6.221 g C m^{-2} yr^{-2}. Thus, human activities dominated ET and GPP trends. As for climatic factors, precipitation and sunshine duration were identified as the major variables regulating ET and GPP trends. For winter wheat–summer maize double cropping system, the increasing trends of ET and GPP mainly

occurred in wheat growing stage; the negative effect of climate change on wheat was less than that on maize; at annual scale, the negative contributions of climate change were offset by the positive contributions of human activities.

Acknowledgment

We thank to all the data providers. We also appreciate editors and reviewers for their constructive comments and suggestions. Finally, the first author is grateful to the invaluable support received from doctoral student ZOU Yi.

References

Bai H Z, Tao F L, Xiao D P *et al.*, 2016. Attribution of yield change for rice-wheat rotation system in China to climate change, cultivars and agronomic management in the past three decades. *Climatic Change*, 135(3): 539–553.

Bai J, Chen X, Li L *et al.*, 2014. Quantifying the contributions of agricultural oasis expansion, management practices and climate change to net primary production and evapotranspiration in croplands in arid northwest China. *Journal of Arid Environments*, 100: 31–41.

Cao G L, Han D M, Song X F, 2014. Evaluating actual evapotranspiration and impacts of groundwater storage change in the North China Plain. *Hydrological Processes*, 28(4): 1797–1808.

Chen B X, Zhang X Z, Tao J *et al.*, 2014. The impact of climate change and anthropogenic activities on alpine grassland over the Qinghai-Tibet Plateau. *Agricultural and Forest Meteorology*, 189: 11–18.

Choudhury B J, DiGirolamo N E, 1998. A biophysical process-based estimate of global land surface evaporation using satellite and ancillary data: I. Model description and comparison with observations. *Journal of Hydrology*, 205(3/4): 164–185.

Dai E F, Huang Y, Wu Z *et al.*, 2016. Analysis of spatio-temporal features of a carbon source/sink and its relationship to climatic factors in the Inner Mongolia grassland ecosystem. *Journal of Geographical Sciences*, 26(3): 297–312.

Dass P, Rawlins M A, Kimball J S *et al.*, 2016. Environmental controls on the increasing GPP of terrestrial vegetation across northern Eurasia. *Biogeosciences*, 13(1): 45–62.

Gao Y N, Yu G R, Yan H M *et al.*, 2014. A MODIS-based Photosynthetic Capacity Model to estimate gross primary production in northern China and the Tibetan Plateau. *Remote Sensing of Environment*, 148: 108–118.

Guo J P, Zhao J F, Wu D R *et al.*, 2014. Attribution of maize yield increase in China to climate change and technological advancement between 1980 and 2010. *Journal of Meteorological Research*, 28(6): 1168–1181.

Jaksa W T, Sridhar V, 2015. Effect of irrigation in simulating long-term evapotranspiration climatology in a human-dominated river basin system. *Agricultural and Forest Meteorology*, 200: 109–118.

Ji X J, Yu Y Q, Zhang W *et al.*, 2010. Spatial-temporal patterns of winter wheat harvest index in China in recent twenty years. *Scientia Agricultura Sinica*, 43(17): 3511–3519. (in Chinese)

Jia Z Z, Liu S M, Xu Z W *et al.*, 2012. Validation of remotely sensed evapotranspiration over the Hai River Basin, China. *Journal of Geophysical Research-Atmospheres*, 117(D13113): 1–21.

Lei H M, Yang D W, 2010. Interannual and seasonal variability in evapotranspiration and energy partitioning over an irrigated cropland in the North China Plain. *Agricultural and Forest Meteorology*, 150(4): 581–589.

Li D, 2014. Assessing the impact of interannual variability of precipitation and potential evaporation on evapotranspiration. *Advances in Water Resources*, 70: 1–11.

Li F Q, Kustas W P, Prueger J H *et al.*, 2005. Utility of remote sensing-based two-source energy balance model under low- and high-vegetation cover conditions. *Journal of Hydrometeorology*, 6(6): 878–891.

Lin Z H, Mo X G, Li H X *et al.*, 2002. Comparison of three spatial interpolation methods for climate variables in China. *Acta Geographica Sinica*, 57(1): 47–56. (in Chinese)

Liu B, Sun Y L, Wang Y C *et al.*, 2013. Monitoring and assessment of vegetation variation in North China based on SPOT/NDVI. *Journal of Arid Land Resources and Environment*, 27(9): 98–103. (in Chinese)

Liu Q A, Yang Z F, 2010. Quantitative estimation of the impact of climate change on actual evapotranspiration in the Yellow River Basin, China. *Journal of Hydrology*, 395(3/4): 226–234.

Liu S M, Xu Z W, Zhu Z L *et al.*, 2013. Measurements of evapotranspiration from eddy-covariance systems and large aperture scintillometers in the Hai River Basin, China. *Journal of Hydrology*, 487: 24–38.

Liu X P, Zhang W J, Yang F *et al.*, 2012. Changes in vegetation-environment relationships over long-term natural restoration process in Middle Taihang Mountain of North China. *Ecological Engineering*, 49: 193–200.

Liu X Y, Li Y Z, Hao W P, 2005. Trend and causes of water requirement of main crops in North China in recent 50 years. *Transactions of the CSAE*, 21(10): 155–159. (in Chinese)

Liu Y A, Wang E L, Yang X G *et al.*, 2010. Contributions of climatic and crop varietal changes to crop production in the North China Plain, since 1980s. *Global Change Biology*, 16(8): 2287–2299.

Liu Z J, Shao Q Q, Liu J Y, 2015. The performances of MODIS-GPP and -ET products in China and their sensitivity to input data (FPAR/LAI). *Remote Sensing*, 7(1): 135–152.

Liu Z J, Wang L C, Wang S S, 2014. Comparison of different GPP models in China using MODIS image and ChinaFLUX data. *Remote Sensing*, 6(10): 10215–10231.

Lobell D B, Asner G P, 2003. Climate and management contributions to recent trends in US agricultural yields. *Science*, 299(5609): 1032–1032.

Lobell D B, Field C B, 2007. Global scale climate-crop yield relationships and the impacts of recent warming. *Environmental Research Letters*, 2(1): 014002.

Lobell D B, Schlenker W, Costa-Roberts J, 2011. Climate trends and global crop production since 1980. *Science*, 333(6042): 616–620.

Ma X N, Zhang M J, Li Y J *et al*., 2012. Decreasing potential evapotranspiration in the Huanghe River Watershed in climate warming during 1960–2010. *Journal of Geographical Sciences*, 22(6): 977–988.

Mo X G, Liu S X, Lin Z H *et al.*, 2011. Patterns of evapotranspiration and GPP and their responses to climate variations over the North China Plain. *Acta Geographica Sinica*, 66(5): 589–598. (in Chinese)

Mo X, Liu S, Lin Z *et al.*, 2015. Trends in land surface evapotranspiration across China with remotely sensed NDVI and climatological data for 1981–2010. *Hydrological Sciences Journal-Journal Des Sciences Hydrologiques*, 60(12): 2163–2177.

Mu Q Z, Zhao M S, Running S W, 2011. Improvements to a MODIS global terrestrial evapotranspiration algorithm. *Remote Sensing of Environment*, 115(8): 1781–1800.

Nicholls N, 1997. Increased Australian wheat yield due to recent climate trends. *Nature*, 387(6632): 484–485.

Qiu G Y, Wang L M, He X H *et al.*, 2008. Water use efficiency and evapotranspiration of winter wheat and its response to irrigation regime in the North China Plain. *Agricultural and Forest Meteorology*, 148(11): 1848–1859.

Savitzky A, Golay M J E, 1964. Smoothing and differentiation of data by simplified least squares procedures. *Analytical Chemistry*, 36(8): 1627–1639.

Shi W J, Tao F L, Zhang Z, 2013. A review on statistical models for identifying climate contributions to crop yields. *Journal of Geographical Sciences*, 23(3): 567–576.

Shi X Y, Mao J F, Thornton P E *et al.*, 2013. Spatiotemporal patterns of evapotranspiration in response to multiple environmental factors simulated by the community land model. *Environmental Research Letters*, 8(2): 024012.

Sun H Y, Liu C M, Zhang X Y *et al.*, 2006. Effects of irrigation on water balance, yield and WUE of winter wheat in the North China Plain. *Agricultural Water Management*, 85(1/2): 211–218.

Sun H Y, Zhang X Y, Wang E L *et al.*, 2016. Assessing the contribution of weather and management to the annual yield variation of summer maize using APSIM in the North China Plain. *Field Crops Research*, 194: 94–102.

Tao F L, Yokozawa M, Liu J Y *et al.*, 2008. Climate-crop yield relationships at provincial scales in China and the impacts of recent climate trends. *Climate Research*, 38(1): 83–94.

Tao F L, Zhang Z, 2013. Climate change, wheat productivity and water use in the North China Plain: A new super-ensemble-based probabilistic projection. *Agricultural and Forest Meteorology*, 170: 146–165.

Turner D P, Ritts W D, Cohen W B *et al.*, 2006. Evaluation of MODIS NPP and GPP products across multiple biomes. *Remote Sensing of Environment*, 102(3/4): 282–292.

Ukkola A M, Prentice I C, 2013. A worldwide analysis of trends in water-balance evapotranspiration. *Hydrology and Earth System Sciences*, 17(10): 4177–4187.

Veron S R, de Abelleyra D, Lobell D B, 2015. Impacts of precipitation and temperature on crop yields in the Pampas. *Climatic Change*, 130(2): 235–245.

Wang H S, Jia G S, Fu C B *et al.*, 2010. Deriving maximal light use efficiency from coordinated flux measurements and satellite data for regional gross primary production modeling. *Remote Sensing of Environment*, 114(10): 2248–2258.

Wang P T, Yan J P, Jiang C *et al.*, 2014. Spatial and temporal variations of reference crop evapotranspiration and its influencing factors in the North China Plain. *Acta Ecologica Sinica*, 34(19): 5589–5599. (in Chinese)

Wang S S, Mo X G, 2015. Comparison of multiple models for estimating gross primary production using remote sensing data and fluxnet observations. *Remote Sensing and GIS for Hydrology and Water Resources*, 368: 75–80.

Wang Z, Ye T, Wang J *et al.*, 2016. Contribution of climatic and technological factors to crop yield: Empirical evidence from late paddy rice in Hunan Province, China. *Stochastic Environmental Research and Risk Assessment*, 30(7): 2019–2030.

Xiao D P, Tao F L, 2014. Contributions of cultivars, management and climate change to winter wheat yield in the North China Plain in the past three decades. *European Journal of Agronomy*, 52: 112–122.

Xiao J F, Zhou Y, Zhang L, 2015. Contributions of natural and human factors to increases in vegetation productivity in China. *Ecosphere*, 6(11): 1–20.

Xiao J F, Zhuang Q L, Law B E *et al*., 2010. A continuous measure of gross primary production for the conterminous United States derived from MODIS and AmeriFlux data. *Remote Sensing of Environment*, 114(3): 576–591.

Xie G H, Han D Q, Wang X Y *et al*., 2011. Harvest index and residue factor of cereal crops in China. *Journal of China Agricultural University*, 16(1): 1–8. (in Chinese)

Zhang S H, Liu S X, Mo X G *et al.*, 2010. Assessing the Impact of Climate Change on Reference Evapotranspiration in Aksu River Basin. *Acta Geographica Sinica*, 65(11): 1363–1370. (in Chinese)

Zhang X Y, Chen S Y, Sun H Y *et al.*, 2011. Changes in evapotranspiration over irrigated winter wheat and maize in North China Plain over three decades. *Agricultural Water Management*, 98(6): 1097–1104.

Zhang X Y, Wang S F, Sun H Y *et al.*, 2013. Contribution of cultivar, fertilizer and weather to yield variation of winter wheat over three decades: A case study in the North China Plain. *European Journal of Agronomy*, 50: 52–59.

Zhang Y J, Xu M, Chen H *et al*., 2009. Global pattern of NPP to GPP ratio derived from MODIS data: Effects of ecosystem type, geographical location and climate. *Global Ecology and Biogeography*, 18(3): 280–290.

Zhang Y L, Song C H, Sun G *et al.*, 2016. Development of a coupled carbon and water model for estimating global gross primary productivity and evapotranspiration based on eddy flux and remote sensing data. *Agricultural and Forest Meteorology*, 223: 116–131.

Zhang Y Q, Yu Q, Jiang J *et al.*, 2008. Calibration of Terra/MODIS gross primary production over an irrigated cropland on the North China Plain and an alpine meadow on the Tibetan Plateau. *Global Change Biology*, 14(4): 757–767.

Zhu X J, Yu G R, Hu Z M *et al.*, 2015. Spatiotemporal variations of T/ET (the ratio of transpiration to evapotranspiration) in three forests of eastern China. *Ecological Indicators*, 52: 411–421.